JACS
JOURNAL OF THE AMERICAN CHEMICAL SOCIETY

Communication

pubs.acs.org/JACS

Gold–Thiolate Ring as a Protecting Motif in the $Au_{20}(SR)_{16}$ Nanocluster and Implications

Chenjie Zeng,[†] Chong Liu,[‡] Yuxiang Chen,[†] Nathaniel L. Rosi,[‡] and Rongchao Jin*,[†]

[†]Department of Chemistry, Carnegie Mellon University, Pittsburgh, Pennsylvania 15213, United States

[‡]Department of Chemistry, University of Pittsburgh, Pittsburgh, Pennsylvania 15213, United States

Supporting Information

ABSTRACT: Understanding how gold nanoclusters nucleate from $Au^{I}SR$ complexes necessitates the structural elucidation of nanoclusters with decreasing size. Toward this effort, we herein report the crystal structure of an ultrasmall nanocluster formulated as $Au_{20}(TBBT)_{16}$ (TBBT = SPh-*t*-Bu). The structure features a vertex-sharing bitetrahedral Au_7 kernel and an unprecedented "ring" motif—$Au_8(SR)_8$. This large ring protects the Au_7 kernel through strong Au_{ring}–Au_{kernel} bonding but does not involve S–Au_{kernel} bonding, in contrast to the common "staple" motifs in which the S–Au_{kernel} bonding is dominant but the Au_{staple}–Au_{kernel} interaction is weak (i.e., aurophilic). As the smallest member in the TBBT "magic series", $Au_{20}(TBBT)_{16}$, together with $Au_{28}(TBBT)_{20}$, $Au_{36}(TBBT)_{24}$, and $Au_{44}(TBBT)_{28}$, reveals remarkable size-growth patterns in both geometric structure and electronic nature. Moreover, $Au_{20}(TBBT)_{16}$, together with the $Au_{24}(SR)_{20}$ and $Au_{18}(SR)_{14}$ nanoclusters, forms a "4e" nanocluster family, which illustrates a trend of shrinkage of bitetrahedral kernels from Au_8^{4+} to Au_7^{3+} and possibly to Au_6^{2+} with decreasing size.

Ligand-protected gold nanoclusters have attracted significant research interest in recent years,[1−8] and various applications of this new class of nanomaterial have been developed, such as catalysis, biomedicine, renewable energy, chemical sensing, etc.[9−12] For thiolate-protected $Au_n(SR)_m$ nanoclusters, a common structural picture has been established:[1] i.e., each size consisting a polyhedron-based gold kernel protected by $Au_x(SR)_{x+1}$ "staple" motifs.[13] Recent efforts have led to a few new crystal structures of $Au_n(SR)_m$ nanoclusters,[5,7,14−16] as well as Au–Cu bimetal nanoclusters[6] and the selenolate-protected gold nanoclusters.[17] One of the important tasks is to understand how the structural evolution from gold–thiolate complexes to gold nanoclusters occurs (i.e., nucleation from the Au(I)SR complex). This goal requires the attainment of nanoclusters with decreasing size.[18−22] While several magic sizes on the smaller end were discovered a long time ago,[18,19] such as $Au_{15}(SR)_{13}$, $Au_{18}(SR)_{14}$, and $Au_{20}(SR)_{16}$, their crystal structures have not been attained, although theoretical calculations have been performed to predict their structures.[20,21,23−26]

Another major question for $Au_n(SR)_m$ nanoclusters pertains to the origin of magic sizes—i.e., why they are stable. A popular explanation is the "noble gas superatom" model, i.e., stable nanoclusters are considered to be analogous to electron-shell closed noble gas atoms, hence nanoclusters with 2e, 8e, 18e, 34e, 58e, 92e, ... should be stable.[27] The superatom model works well in gas-phase bare metal clusters, as demonstrated long before,[28] but does not seem to work equally well in the case of solution-phase ligand-protected $Au_n(SR)_m$ nanoclusters.[5,29] One of the typical superatoms is $Au_{25}(SR)_{18}^{-}$, which possesses 8e and would be expected to be chemically inert like noble gas atoms, but $Au_{25}(SR)_{18}^{-}$ is indeed quite reactive (e.g., spontaneous one-electron loss in air and conversion to the 7e $[Au_{25}(SR)_{18}]^0$ stable radical).[29,30] Another two 8e nanoclusters, $Au_{23}(SR)_{16}^{-}$ and $Au_{28}(SR)_{20}$, are non-spherical and hence non-superatoms.[5,15] Given the limitations of the simple superatom model, theoretical efforts[31−35] have been made to accommodate nonspherical shapes and develop new models such as "superatom molecules" and "superatom network"—which have been put forth in an attempt to explain the electronic structure of some stable $Au_n(SR)_m$ nanoclusters. To further understand the issue of what determines the stability of $Au_n(SR)_m$ nanoclusters, major efforts in both experiment and theory are still needed.

Here we report the crystal structure of the chiral $Au_{20}(TBBT)_{16}$ nanocluster (TBBT = SPh-*t*-Bu), which comprises a Au_7 kernel and surface protecting motifs of monomeric and trimeric staples as well as the first observed $Au_8(SR)_8$ ring motif (Figure 1). This structure together with its "relatives"

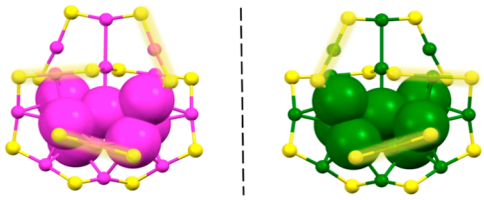

Figure 1. X-ray structure of the two enantiomers of chiral $Au_{20}(TBBT)_{16}$. Color codes: magenta/green, gold atoms in different enantiomers; yellow, sulfur. The Ph-*t*-Bu tails are omitted for clarity.

$Au_{28}(TBBT)_{20}$, $Au_{36}(TBBT)_{24}$, and $Au_{44}(TBBT)_{28}$[14,15,36] provide important implications for the fundamental issues of the $Au^{I}SR$ complex to nanocluster transition (i.e., the nucleation behavior), the growth pattern, and the electronic structure evolution.

The $Au_{20}(TBBT)_{16}$ nanocluster was synthesized by a ligand-exchange-induced size/structure transformation reaction (yield

Received: July 6, 2014
Published: August 15, 2014

   dx.doi.org/10.1021/ja506802n | *J. Am. Chem. Soc.* 2014, 136, 11922−11925

~10%).[14,15,37] The present case involves thermal reaction of $Au_{25}(SC_2H_4Ph)_{18}$ with excess 4-*tert*-butylbenzenethiol at 40 °C (see the Supporting Information for details). The large excess of TBBT thiol (i.e., 150:1 molar ratio of TBBT to SC_2H_4Ph in $Au_{25}(SC_2H_4Ph)_{18}$) facilitated the complete replacement of SC_2H_4Ph with TBBT in the nanoclusters. Single-crystal growth was performed via vapor diffusion of pentane into a CH_2Cl_2 solution of nanoclusters. Needlelike dark orange single crystals were obtained. The $Au_{20}(TBBT)_{16}$ nanoclusters crystallize in the enantiomorphic space group $P222_1$. The two enantiomers in the unit cell (Figure S1, Supporting Information) are highlighted in green and magenta, respectively. Below, we choose one of the enantiomers for detailed structural analysis.

The structure of $Au_{20}(TBBT)_{16}$ features an unique vertex-sharing bitetrahedral Au_7 kernel (Figure 2A, magenta).

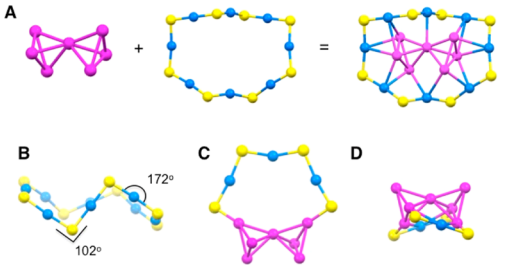

Figure 2. Anatomy of the structure of $Au_{20}(TBBT)_{16}$: (A) Au_7 kernel and the octameric ring motif; (B) chair conformation of the octameric ring; (C, D) trimeric and monomeric staple motifs. Color codes: magenta, Au in the kernel; blue, Au on the surface; yellow, S.

Remarkably, a giant $Au_8(SR)_8$ octameric ring (Figure 2A, middle) is discovered, which circles the Au_7 kernel (Figure 2A, right). The octameric ring motif adopts a chair conformation (Figure 2B), with average SR–Au^I–SR angle of 172.25 ± 3.89° and Au^I–SR–Au^I angle of 102.11 ± 4.64°. The gold–thiolate ring interacts with the kernel exclusively through Au_{ring}–Au_{kernel} bonding (3.02 ± 0.10 Å)—which is only 4.9% longer than the Au–Au distance of 2.88 Å in bulk gold, indicating strong interaction between the ring and the Au_7 kernel. None of the thiolate ligands in the ring is bonded with the Au atoms of the kernel (Figure 2A). Thus, the interaction mode between the ring and the kernel is in striking contrast with the "clamping" mode which has S–Au_{kernel} bonding between the staple motif and the kernel in the previously reported structures. Thus, the ring motif is distinctly different from the common staple motifs.

The surface-protecting $Au_8(SR)_8$ ring motif is indeed observed for the first time in nanoclusters and can be viewed as a transitional manifestation between Au^ISR complexes and $Au_n(SR)_m$ nanoclusters. It is known that some of the $[Au^ISR]_n$ complexes exhibit ring structures, such as the two pentameric rings in $Au_{10}(TBBT)_{10}$ and two hexameric rings in $Au_{12}(TBBT)_{12}$.[38] On the other hand, $Au_x(SR)_{x+1}$ staple motifs have been found to be "universal" in the nanocluster structures reported so far, and a general trend is that, with decreasing size, the nanocluster exhibits an increasing surface curvature, hence requiring more extended staple motifs for protection.[16,20,21,34] The discovery of a gold–thiolate ring in $Au_{20}(TBBT)_{16}$ indicates that the ring motif might be common in smaller gold nanoclusters such as $Au_{18}(SR)_{14}$ and $Au_{15}(SR)_{13}$.

In addition to the octameric ring, the Au_7 bitetrahedral kernel is further protected by a –SR–Au–SR–Au–SR–Au–SR– trimeric staple (Figure 2C) and two –SR–Au–SR– monomeric staples (Figure 2D). The trimeric staple is planar and clamps onto two vertex Au atoms of the Au_7 bitetrahedron (Figure 2C), whereas the two monomeric staples approach the front and back of the kernel and clamp onto the remaining four vertex Au atoms of the kernel (Figure 2D). The balance between the spatial arrangement of ligands and full protection of the surface of Au_7 kernel gives rise to the unique structure of $Au_{20}(TBBT)_{16}$.

The total structure of $Au_{20}(TBBT)_{16}$ with carbon tails is shown in Figure 3. All of the carbon atoms of the ligands were

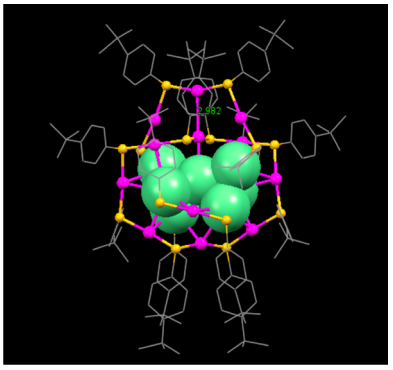

Figure 3. Total structure of one enantiomer of $Au_{20}(TBBT)_{16}$ with the Au_7 kernel shown in space-filling form, the surface protecting motifs in ball and stick form, and the carbon tails in wireframe form.

found in the X-ray crystallographic analysis. The chirality of the nanocluster arises from the peculiar arrangements of the octomeric ring and the trimeric and monomeric staples (Figure 1). It is worth noting that the trimeric staple connects to a gold atom of the ring via a short Au–Au bond (2.982 Å; Figure 3). This bond reduces the swinging flexibility of the trimer and further stablizes the entire particle. We also note that a chiral $Au_{20}(PP_3)_4Cl_4$ nanocluster (where PP_3 refers to a tetradentate phosphine ligand) has been reported recently.[39,40]

The $Au_{20}(TBBT)_{16}$ nanocluster together with the previously reported $Au_{28}(TBBT)_{20}$, $Au_{36}(TBBT)_{24}$, and $Au_{44}(TBBT)_{28}$ forms a neat "magic series" with a uniform $Au_8(TBBT)_4$ progression between adjacent sizes.[14,15,36] The $Au_{20}(TBBT)_{16}$ nanocluster is the smallest member in this magic series. Note that further reduction by $Au_8(TBBT)_4$ would lead to $Au_{12}(TBBT)_{12}$, which is a complex instead of a nanocluster. Naturally, it is of interest to consider the intrinsic relationships among these nanoclusters (vide infra).

First of all, as discussed above, $Au_{20}(TBBT)_{16}$ has a vertex-sharing Au_7 bitetrahedral kernel, in which the two tetrahedra rotate by ~60° with respect to each other to form a staggered configuration (Figure 4A). The Au_7 structure is slightly bent due to the external ring and the staple protecting units, with the top Au–Au edge length being 5.15 Å and two bottom edges being 4.08 Å. Within each tetrahedron of the bitetrahedral kernel, very short Au–Au bond lengths are observed, with an average of 2.72

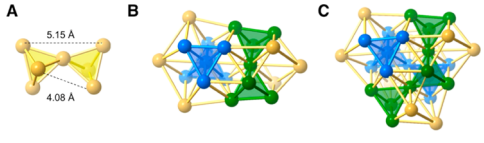

Figure 4. Vertex-sharing tetrahedra in (A) Au_7 kernel of $Au_{20}(TBBT)_{16}$, (B) Au_{20} FCC kernel of $Au_{28}(TBBT)_{20}$, and (C) Au_{28} FCC kernel of $Au_{36}(TBBT)_{24}$.

dx.doi.org/10.1021/ja506802n | J. Am. Chem. Soc. 2014, 136, 11922–11925

± 0.03 Å (cf. the 2.88 Å Au−Au bond length in bulk gold), indicating strongly bonded individual tetrahedra.

Such a vertex-sharing tetrahedral motif can also be found in the face-centered-cubic (FCC) kernels of $Au_{28}(TBBT)_{20}$ and $Au_{36}(TBBT)_{24}$ (Figure 4B,C).[14,15] In the $Au_{28}(TBBT)_{20}$, a pair of bitetrahedral motifs is identified in the Au_{20} FCC kernel and one bitetrahedron is rotated relative to the other bitetrahedron (Figure 4B, blue vs green).[15] The peculiar tetrahedra in the Au_{20} FCC kernel exhibit much shorter Au−Au bond lengths (2.74 ± 0.03 Å) within each tetrahedron in comparison to the bond lengths outside the tetrahedral unit (3.03 ± 0.03 Å).[15] This significant bond length difference seems to reflect the "nucleation" of tetrahedral units in the FCC kernel of $Au_{28}(TBBT)_{20}$. Similarly, for $Au_{36}(TBBT)_{24}$, a pair of vertex-sharing tritetrahedral units can be identified (Figure 4C, blue vs green), and the average Au−Au bond length is 2.78 ± 0.06 Å (within the tetrahedron) and 3.00 ± 0.07 Å (outside the tetrahedron).[14] Note that Chevrier et al. reported the pseudo Au_4 units in $Au_{36}(TBBT)_{24}$ through X-ray absorption spectroscopic analysis.[41] Knoppe et al.[33] and Pei et al.[35] also interpreted tetrahedron-based kernels of $Au_{28}(TBBT)_{20}$, $Au_{36}(TBBT)_{24}$, and $Au_{44}(TBBT)_{28}$ through theoretical analyses. In our present work, the vertex-sharing Au_7 bitetrahedral kernel discovered in the $Au_{20}(TBBT)_{16}$ nanocluster serves as a basic structure unit and reveals the intrinsic structural relationship in the magic series of TBBT-protected nanoclusters and also sheds light on the nucleation and growth behavior.

Secondly, this magic series provides insights into the electronic structure relationship. On the basis of the electron-counting rules (i.e., each gold atom in $Au_n(SR)_m$ contributes one Au(6s) free electron and each thiolate ligand localizes one electron), $Au_{20}(TBBT)_{16}$, $Au_{28}(TBBT)_{20}$, $Au_{36}(TBBT)_{24}$, and $Au_{44}(TBBT)_{28}$ have formally 4e, 8e, 12e, and 16e, respectively. It is intriguing that, with each increment of 4e, a stable magic size forms. This trend does not follow the "superatom" model (i.e., 2e, 8e, 18e, 34e, 58e, ...). One reason is that the superatom model is based on spherical shell-by-shell electron filling, while the $Au_n(TBBT)_m$ magic series grows in size through successively adding tetrahedral units; thus, rather than resembling the noble-gas *atoms*, the $Au_n(TBBT)_m$ series resembles the more complex case of *multiatom molecules*, such as the series of conjugated molecules butadiene, octatetraene, etc. Assuming that each tetrahedral unit requires two Au(6s) electrons as "glue" (i.e., delocalized Au−Au bonds within the tetrahedron, Au_4^{2+}), the number of electrons in each size of the magic series is equal to twice the number of tetrahedral units: for example, 4e for the two tetrahedra in $Au_{20}(TBBT)_{16}$, 8e for four tetrahedra in $Au_{28}(TBBT)_{20}$, etc. Of note, the phosphine-protected Au_4^{2+} cluster was reported before and its electronic configuration was proposed.[42−44]

The $Au_{20}(TBBT)_{16}$ shows the harmony between its geometric and electronic requirements. The Au_7 vertex-sharing bitetrahedral kernel requires three staple motifs to protect the six exposed gold atoms (note that each staple motif has two sulfur ends and thus can protect two gold atoms). On the other hand, the Au_7 kernel only supports four free electrons, and the remaining three Au(6s) electrons need to be localized by thiolates, which necessitates bonding to three staples to form a Au_7^{3+} kernel (note that each staple motif can only localize one electron due to the 0.5 bond order in the −S(R)− bridging mode). In the structure of $Au_{20}(TBBT)_{16}$, three staple motifs (including one trimeric staple and two monomeric staples) protect the Au_7 kernel, and the remaining eight gold atoms and eight thiolates form a ring structure to wrap the kernel and do not require additional "footholds" on the kernel, nor does the ring localize additional Au(6s) valence electrons in the kernel. The ring motif is a "smart" strategy adopted in ultrasmall nanoclusters for accommodating extra gold atoms and thiolate ligands to build robust structures.

Thirdly, the $Au_{20}(TBBT)_{16}$ is also a member of the "isoelectron" 4e nanocluster family, including $Au_{18}(SR)_{14}$ and $Au_{24}(SR)_{20}$.[45−47] More insights into the structures of ultrasmall nanoclusters can be gained by comparing $Au_{20}(TBBT)_{16}$ with the reported structures of $Au_{24}(SCH_2Ph\text{-}t\text{-}Bu)_{20}$ and $Au_{24}(SePh)_{20}$.[16,17] As shown in Figure 5A,B, the kernels of

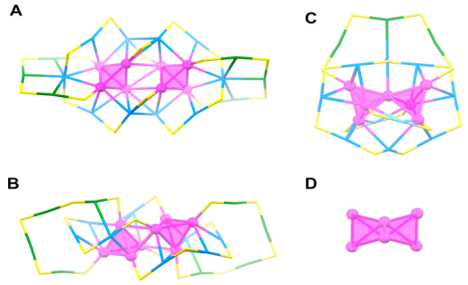

Figure 5. "4e" nanoclusters with different gold kernels and protecting motifs: (A) $Au_{24}(SePh)_{20}$; (B) $Au_{24}(SCH_2Ph\text{-}t\text{-}Bu)_{20}$; (C) $Au_{20}(TBBT)_{16}$; (D) the proposed edge-sharing Au_6^{2+} bitetrahedral kernel in $Au_{18}(SR)_{14}$. Color codes: magenta, kernel Au atoms; green/blue, surface Au atoms; yellow, sulfur.

$Au_{24}(S/Se\text{-}R)_{20}$ are also composed of two tetrahedra, but the two tetrahedra within each Au_8^{4+} kernel are quite independent of each other, as reflected in the long Au−Au distances between individual tetrahedra,[16,17] in contrast to the vertex-sharing bitetrahedral Au_7^{3+} kernel in $Au_{20}(TBBT)_{16}$ (Figure 5C). Note that the two independent tetrahedra adopt different configurations (Figure 5A,B), and accordingly the bitetrahedral Au_8^{4+} kernel in $Au_{24}(SePh)_{20}$ requires protection by two trimeric and two pentameric staples,[17] while the different Au_8^{4+} kernel in $Au_{24}(SCH_2Ph\text{-}t\text{-}Bu)_{20}$ is protected by four tetrameric staples.[16] In either way, all eight atoms in the Au_8 kernel are exposed and bonded to thiolates in a one-on-one fashion, and four electrons in the Au_8 kernel are thus localized by four staples, forming Au_8^{4+}. Taken together, the size reduction from $Au_{24}(S/Se\text{-}R)_{20}$ to $Au_{20}(SR)_{16}$ is manifested in the shrinkage of the kernel from the bitetrahedral Au_8^{4+} kernel to the vertex-sharing bitetrahedral Au_7^{3+} kernel as well as the introduction of a ring motif in $Au_{20}(SR)_{16}$.

On the basis of the above structural and electronic insights, we predict that the next smaller 4e nanocluster—$Au_{18}(SR)_{14}$—possibly possesses an edge-sharing bitetrahedral Au_6^{2+} kernel (Figure 5D). The exposed four "footholds" in the Au_6 kernel require two staple motifs for protection, which also generate 2+ charges to the kernel. Such an Au_6^{2+} kernel can be found in the phosphine-protected gold cluster.[48] On the basis of the ring and staple motifs, a possible anatomy of the $Au_{18}(SR)_{14}$ formula is predicted to be $Au_6[Au_6(SR)_6][Au_3(SR)_4]_2$. The trend from the Au_8^{4+} to Au_7^{3+} to Au_6^{2+} bitetrahedral kernels corresponding to $Au_{24}(SR)_{20}$, $Au_{20}(SR)_{16}$, and $Au_{18}(SR)_{14}$, respectively, is different from the previous theoretical calculations—which involve the bitetrahedral Au_8^{4+} kernel exclusively as a prototype for all of these 4e nanoclusters. Specifically, Pei et al. and Jiang et al. predicted the $Au_{20}(SR)_{16}$ structure as $Au_8[Au_3(SR)_4]_4$.[20,21] Tlahuice et al. calculated the $Au_{18}(SR)_{14}$ structure as $Au_8[Au_2(SR)_3]_2[Au_3(SR)_4]_2$.[23] Cheng et al. calculated the

dx.doi.org/10.1021/ja506802n | J. Am. Chem. Soc. 2014, 136, 11922−11925

three nanoclusters' structures on the basis of the Au_8^{4+} kernel.[31] The vertex-sharing bitetrahedral Au_7^{3+} kernel discovered in the present $Au_{20}(TBBT)_{16}$ illustrates that, as the number of atoms decreases from Au_8 to Au_7 in the kernel, tighter connection between tetrahedral units is manifested: that is, from no vertex sharing in the Au_8 kernel to one-vertex sharing in the Au_7 kernel. Accordingly, an even tighter edge-sharing Au_6^{2+} kernel is predicted to be possibly present in the $Au_{18}(SR)_{14}$ nanocluster.

In summary, the ring motif discovered in $Au_{20}(TBBT)_{16}$ may imply the prevalence of this new type of surface-protecting motif in small nanoclusters, and the tetrahedral packing mode in the kernel also illustrates the trend from Au_8^{4+} (in $Au_{24}(SR)_{20}$) to Au_7^{3+} (in $Au_{20}(SR)_{16}$) and inspires us to predict a possible Au_6^{2+} kernel in the smaller $Au_{18}(SR)_{14}$ nanocluster. Future work on the structures of $Au_n(SR)_m$ nanoclusters with decreasing size is expected to reveal more details on the critical transition from Au^ISR complexes to the $Au_n(SR)_m$ nanoclusters, including the nucleation behavior of the Au kernel out of the Au^ISR complex and the generality of the ring motif. The diverse structures of gold nanoclusters may evoke the multiatomic molecule picture, which has a higher level of complexity than simple superatoms.

■ ASSOCIATED CONTENT

Supporting Information

Text giving details of the synthesis, crystallization, and X-ray analysis and a figure, tables, and a CIF file showing the unit cell packing, structural parameters, and crystallographic data for $Au_{20}(TBBT)_{16}$. This material is available free of charge via the Internet at http://pubs.acs.org.

■ AUTHOR INFORMATION

Corresponding Author

*E-mail for R.J.: rongchao@andrew.cmu.edu.

Notes

The authors declare no competing financial interest.

■ ACKNOWLEDGMENTS

This work was supported by the Air Force Office of Scientific Research under AFOSR Award No. FA9550-11-1-9999 (FA9550-11-1-0147) and the Camille Dreyfus Teacher-Scholar Awards Program.

■ REFERENCES

(1) Qian, H.; Zhu, M.; Wu, Z.; Jin, R. *Acc. Chem. Res.* **2012**, *45*, 1470.
(2) Kamei, Y.; Shichibu, Y.; Konishi, K. *Angew. Chem., Int. Ed.* **2011**, *50*, 7442.
(3) Wan, X.-K.; Lin, Z.-W.; Wang, Q.-M. *J. Am. Chem. Soc.* **2012**, *134*, 14750.
(4) Chen, J.; Zhang, Q.-F.; Bonaccorso, T. A.; Williard, P. G.; Wang, L.-S. *J. Am. Chem. Soc.* **2013**, *136*, 92.
(5) Das, A.; Li, T.; Nobusada, K.; Zeng, C.; Rosi, N. L.; Jin, R. *J. Am. Chem. Soc.* **2013**, *135*, 18264.
(6) Yang, H.; Wang, Y.; Yan, J.; Chen, X.; Zhang, X.; Häkkinen, H.; Zheng, N. *J. Am. Chem. Soc.* **2014**, *136*, 7197.
(7) Crasto, D.; Malola, S.; Brosofsky, G.; Dass, A.; Häkkinen, H. *J. Am. Chem. Soc.* **2014**, *136*, 5000.
(8) Maity, P.; Takano, S.; Yamazoe, S.; Wakabayashi, T.; Tsukuda, T. *J. Am. Chem. Soc.* **2013**, *135*, 9450.
(9) Li, G.; Zeng, C.; Jin, R. *J. Am. Chem. Soc.* **2014**, *136*, 3673.
(10) Zhang, X.-D.; Luo, Z.; Chen, J.; Shen, X.; Song, S.; Sun, Y.; Fan, S.; Fan, F.; Leong, D. T.; Xie, J. *Adv. Mater.* **2014**, *26*, 4565.
(11) Chen, Y.-S.; Choi, H.; Kamat, P. V. *J. Am. Chem. Soc.* **2013**, *135*, 8822.
(12) Wu, Z.; Wang, M.; Yang, J.; Zheng, X.; Cai, W.; Meng, G.; Qian, H.; Wang, H.; Jin, R. *Small* **2012**, *8*, 2028.
(13) Pei, Y.; Pal, R.; Liu, C.; Gao, Y.; Zhang, Z.; Zeng, X. C. *J. Am. Chem. Soc.* **2012**, *134*, 3015.
(14) Zeng, C.; Qian, H.; Li, T.; Li, G.; Rosi, N. L.; Yoon, B.; Barnett, R. N.; Whetten, R. L.; Landman, U.; Jin, R. *Angew. Chem., Int. Ed.* **2012**, *51*, 13114.
(15) Zeng, C.; Li, T.; Das, A.; Rosi, N. L.; Jin, R. *J. Am. Chem. Soc.* **2013**, *135*, 10011.
(16) Das, A.; Li, T.; Li, G.; Nobusada, K.; Zeng, C.; Rosi, N. L.; Jin, R. *Nanoscale* **2014**, *6*, 6458.
(17) Song, Y.; Wang, S.; Zhang, J.; Kang, X.; Chen, S.; Li, P.; Sheng, H.; Zhu, M. *J. Am. Chem. Soc.* **2014**, *136*, 2963.
(18) Negishi, Y.; Nobusada, K.; Tsukuda, T. *J. Am. Chem. Soc.* **2005**, *127*, 5261.
(19) Zhu, M.; Qian, H.; Jin, R. *J. Am. Chem. Soc.* **2009**, *131*, 7220.
(20) Pei, Y.; Gao, Y.; Shao, N.; Zeng, X. C. *J. Am. Chem. Soc.* **2009**, *131*, 13619.
(21) Jiang, D.-e.; Chen, W.; Whetten, R. L.; Chen, Z. *J. Phys. Chem. C* **2009**, *113*, 16983.
(22) Yao, Q.; Yu, Y.; Yuan, X.; Yu, Y.; Xie, J.; Lee, J. Y. *Small* **2013**, *9*, 2696.
(23) Tlahuice, A.; Garzon, I. L. *Phys. Chem. Chem. Phys.* **2012**, *14*, 3737.
(24) Jiang, D.-e.; Overbury, S. H.; Dai, S. *J. Am. Chem. Soc.* **2013**, *135*, 8786.
(25) Tlahuice-Flores, A.; Jose-Yacaman, M.; Whetten, R. L. *Phys. Chem. Chem. Phys.* **2013**, *15*, 19557.
(26) Yu, Y.; Luo, Z.; Chevrier, D. M.; Leong, D. T.; Zhang, P.; Jiang, D.-e.; Xie, J. *J. Am. Chem. Soc.* **2014**, *136*, 1246.
(27) Walter, M.; Akola, J.; Lopez-Acevedo, O.; Jadzinsky, P. D.; Calero, G.; Ackerson, C. J.; Whetten, R. L.; Grönbeck, H.; Häkkinen, H. *Proc. Natl. Acad. Sci. U.S.A.* **2008**, *105*, 9157.
(28) Martin, T. P.; Bergmann, T.; Gohlich, H.; Lange, T. *J. Phys. Chem.* **1991**, *95*, 6421.
(29) Zhu, M.; Eckenhoff, W. T.; Pintauer, T.; Jin, R. *J. Phys. Chem. C* **2008**, *112*, 14221.
(30) Zhu, M.; Aikens, C. M.; Hendrich, M. P.; Gupta, R.; Qian, H.; Schatz, G. C.; Jin, R. *J. Am. Chem. Soc.* **2009**, *131*, 2490.
(31) Cheng, L.; Yuan, Y.; Zhang, X.; Yang, J. *Angew. Chem., Int. Ed.* **2013**, *52*, 9035.
(32) Cheng, L.; Ren, C.; Zhang, X.; Yang, J. *Nanoscale* **2013**, *5*, 1475.
(33) Knoppe, S.; Malola, S.; Lehtovaara, L.; Bürgi, T.; Häkkinen, H. *J. Phys. Chem. A* **2013**, *117*, 10526.
(34) Jiang, D.-e. *Nanoscale* **2013**, *5*, 7149.
(35) Pei, Y.; Lin, S.; Su, J.; Liu, C. *J. Am. Chem. Soc.* **2013**, *135*, 19060.
(36) Zeng, C.; Chen, Y.; Li, G.; Jin, R. *Chem. Commun.* **2014**, *50*, 55.
(37) Zeng, C.; Liu, C.; Pei, Y.; Jin, R. *ACS Nano* **2013**, *7*, 6138.
(38) Wiseman, M. R.; Marsh, P. A.; Bishop, P. T.; Brisdon, B. J.; Mahon, M. F. *J. Am. Chem. Soc.* **2000**, *122*, 12598.
(39) Wan, X.-K.; Yuan, S.-F.; Lin, Z.-W.; Wang, Q.-M. *Angew. Chem., Int. Ed.* **2014**, *53*, 2923.
(40) Chen, J.; Zhang, Q.-F.; Williard, P. G.; Wang, L.-S. *Inorg. Chem.* **2014**, *53*, 3932.
(41) Chevrier, D. M.; Chatt, A.; Zhang, P.; Zeng, C.; Jin, R. *J. Phys. Chem. Lett.* **2013**, *4*, 3186.
(42) Evans, D. G.; Mingos, D. M. P. *J. Organomet. Chem.* **1982**, *232*, 171.
(43) Hudgens, J. W.; Pettibone, J. M.; Senftle, T. P.; Bratton, R. N. *Inorg. Chem.* **2011**, *50*, 10178.
(44) Ivanov, S. A.; Arachchige, I.; Aikens, C. M. *J. Phys. Chem. A* **2011**, *115*, 8017.
(45) Zhu, M.; Qian, H.; Jin, R. *J. Phys. Chem. Lett.* **2010**, *1*, 1003.
(46) Yu, Y.; Chen, X.; Yao, Q.; Yu, Y.; Yan, N.; Xie, J. *Chem. Mater.* **2013**, *25*, 946.
(47) Xu, Q.; Wang, S.; Liu, Z.; Xu, G.; Meng, X.; Zhu, M. *Nanoscale* **2013**, *5*, 1176.
(48) Briant, C. E.; Hall, K. P.; Mingos, D. M. P.; Wheeler, A. C. *J. Chem. Soc., Dalton Trans.* **1986**, 687.